IEEE Access
Multidisciplinary | Rapid Review | Open Access Journal

Received November 8, 2020, accepted December 9, 2020, date of publication December 15, 2020,
date of current version December 30, 2020.

Digital Object Identifier 10.1109/ACCESS.2020.3044909

Adaptive Potential Field-Based Path Planning for Complex Autonomous Driving Scenarios

BING LU[1], GUOFA LI[2], (Member, IEEE), HUILONG YU[3], (Member, IEEE), HONG WANG[4], JINQUAN GUO[1], DONGPU CAO[3], AND HONGWEN HE[1], (Senior Member, IEEE)

[1]National Engineering Laboratory for Electric Vehicles, Beijing Institute of Technology, Beijing 100081, China
[2]College of Mechatronics and Control Engineering, Shenzhen University, Shenzhen 518060, China
[3]Department of Mechanical and Mechatronics Engineering, Waterloo University, Waterloo, ON N2L 3G1, Canada
[4]Tsinghua Intelligent Vehicle Design and Safety Research Institute, Tsinghua University, Beijing 100084, China

Corresponding authors: Hongwen He (hwhebit@bit.edu.cn) and Huilong Yu (huilong.yu@ieee.org)

This work was supported in part by the National Key Research and Development Program of China under Grant 2018YFB0106200, and in part by the National Science Foundation of China Joint Fund Project under Grant U1864205.

ABSTRACT An adaptive potential field is designed to adapt the acceleration/deceleration and mass of the obstacle. The potential fields are established in a transformed road coordinate system to improve the feasibility and robustness. A path planning method is proposed based on the designed adaptive potential field to improve the driving safety and the ride comfort of autonomous vehicles in complex driving scenarios, which including the cut-in, emergency braking, obstacle sudden accelerating during overtaking and the curve road driving scenarios. The effectiveness of the proposed method is validated by simulations with constructed and real data, respectively. The *TTC*s (Time-to-Collision) and the maximum lateral accelerations are used to evaluate the improvements on safety and ride comfort. The results show that both the driving safety and ride comfort are efficiently improved by using the proposed approach in emergency braking and accelerating scenarios. Meanwhile, the proposed method can be well applied in a curve road driving environment.

INDEX TERMS Autonomous vehicles, adaptive potential field, path planning, complex driving scenario, model predictive control.

I. INTRODUCTION

A. MOTIVATION

Path planning as an important component of autonomous driving techniques has been widely researched in recent years [1]. Various algorithms have been developed for path planning according to the application scenarios [2], e.g. RRT methods for structured [3] and unstructured driving scenarios [4], A* algorithm for off-line path planning [5], [6], polynomial interpolation approaches for real-time motion planning [7], etc. Meanwhile, the driving safety is essential for autonomous driving which should be ensured and improved [8]. Considering the improvements on driving safety during obstacle avoidance, the potential field-based approaches have been popularly used for path planning of autonomous vehicles (AVs) [9].

The main idea behind the conventional potential field-based path planning (CPF-PP) is to design a repulsive potential field (PF) around the obstacle and an attractive PF around a target point [10], respectively. The repulsive PF will enforce the approaching vehicles keep a safe distance to the obstacle for avoiding collision [11]. Being different from the function of repulsive PF, the attractive PF is constructed to lead the ego vehicle driving towards the target position [12]. Road boundaries are also handled with the repulsive PF to prevent the ego vehicle driving out of the road edges. Based on the repulsive and attractive PFs, there are usually two methods for path generation under different application situations, i.e. the generated route with minimum PF [13] and the generated route along the descent direction of PF's gradient [14]. The former method depends on the constructed repulsive and attractive PFs and can be uniquely generated when the positions of obstacles are determined. Combining with the nonholonomic constraints, the latter method is usually to sampling along the descent direction of PF's gradient to generate a drivable reference path [15]. Furthermore, the PFs can also be independently applied as driving safety fields for the risk assessment of autonomous

The associate editor coordinating the review of this manuscript and approving it for publication was Moussa Boukhnifer.

driving [16]. According to the definition of safety field, the PF values around the obstacles are used to declare the risk degree of collision [17]. However, these applications of the PF are based on the assumption that the shape of the PFs are symmetric distribution [18], and the PFs are only constructed and applied in a straight road environment. While driving on curve roads, the performances of previous PFs methods may not be ensured, which will result in the failure of AVs to acquire the expected trajectory and thus a traffic accident may occur. Therefore, an appropriate design of PF needs to be examined on both straight and curve road environment to demonstrate the effectiveness of the proposed method in various situations.

Meanwhile, the collision risk of an obstacle to the subject vehicle is different when it is with different position (e.g., in the front or rear) from the subject vehicle. For example, its rear vehicle will take an emergency braking or sharp steering for safety when a vehicle suddenly decelerates, while its front vehicle will not be influenced. This phenomenon indicates that the dangerous degree in the rear of the obstacle vehicle is higher than that of the front when the obstacle vehicle is decelerating [19]. Similarly, the left side of the obstacle has a higher collision risk than that of the right side in the left steering process of the obstacle [20]. These indicate that the collision risk around an obstacle is not symmetric distribution when the obstacle is accelerating/decelerating. Furthermore, the collision risk can be influenced by the mass of the obstacle as well, e.g. the collision risk of the rock to the vehicle is obviously higher than that of the same sized plastic box to the vehicle. These illustrate the acceleration/deceleration and the mass of an obstacle should be taken into consideration for the PF definition.

Therefore, an adaptive potential field (ADPF) method is proposed in this paper by comprehensively considering the mass and acceleration/deceleration behavior of the obstacle and the road curvature. It is expected that the proposed ADPF will be more mimic to the practical driving scenarios, and the robustness and feasibility of the path planning approach will be improved for autonomous driving. To examine its effectiveness and to evaluate the improvements of the proposed algorithm, three typical complex traffic scenarios are constructed. Furthermore, a crowd highway scenario with real information of surrounding vehicles is extracted from the highD dataset [21] for further validation.

B. CONTRIBUTIONS

1) A novel adaptive potential field is designed to adapt the vary of acceleration/deceleration and mass of the obstacles. The dynamic feature of ADPF can be well used to present the intention of the obstacle to mimic the practical driving situation.
2) The ADPF-based path planning (ADPF-PP) is proposed to improve the driving safety and ride comfort of the autonomous vehicles in various scenarios including emergency braking, fast cut-in, and sudden acceleration of the obstacle vehicle.
3) A road coordinate system is transformed and used to establish the PFs, which makes the proposed ADPF-PP useful for both straight road and curve road scenarios. To the best of our knowledge, this is one of the first attempts to apply innovatively proposed potential field-based methods in curve road scenarios.

C. PAPER ORGANIZATION

This paper is organized as follows: The adaptive potential field of the obstacle is designed in Section II. Section III introduces the path planning process based on the ADPF. Various driving scenarios are constructed for path planning and tracking simulation in Section IV to examine the effectiveness and improvements of proposed algorithm. Finally, the conclusions are presented in Section V.

II. THE DESIGN OF ADAPTIVE POTENTIAL FIELD IN ROAD COORDINATE SYSTEM

The vehicle position can be described with a static Cartesian coordinate (X_o, Y_o) or a moving road coordinate (s_o, d_o) as illustrated in Fig.1. The on-board positioning system (GPS/BeiDou) of AVs can directly obtain the current position of the vehicle in the world Cartesian coordinate system. To detect whether a lane departure is happening, the relative position of the ego vehicle to the centre line of the target lane is required to calculated in real-time with a road coordinate system.

A. A ROAD COORDINATE

Based on the Frenet-Serret formulas [22], a moving road coordinate is transformed with the Cartesian coordinates of a given road. Fig.1 indicates that the descriptions of the relative position between the ego vehicle and obstacle in two coordinate systems are different as (1) and (2).

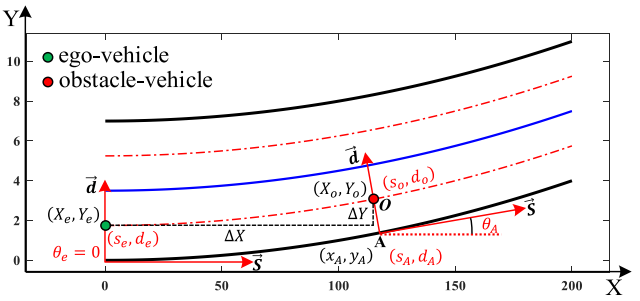

FIGURE 1. Descriptions of relative positions in different coordinate systems.

In global Cartesian coordinate system ($X \perp Y$):

$$\begin{cases} \Delta X = |X_o - X_e| \\ \Delta Y = |Y_o - Y_e|. \end{cases} \tag{1}$$

In a moving road coordinate system ($\vec{s} \perp \vec{d}$):

$$\begin{cases} \Delta s = |s_o - s_e| \\ \Delta d = |d_o - d_e|, \end{cases} \tag{2}$$

where $\vec{s}$ and $\vec{d}$ are the tangential and normal directions in the road coordinate, Δs and Δd denote the relative distances between the ego vehicle and obstacle vehicle in the two orthogonal directions of the road coordinate, respectively.

B. COORDINATE TRANSFORMATION

1) GLOBAL X-Y TO MOVING ROAD S-D COORDINATE

For coordinate transformation purpose, the given path should satisfy the drivable characteristics described as

$$\begin{cases} \forall x \in \mathbb{R} \\ \exists : x \to y = f(x) \\ \quad x \to \dot{f}(x), x \to \ddot{f}(x). \end{cases} \tag{3}$$

The arc length (S) is monotonically increasing and can be calculated by

$$S(x, y) = \int_{x_0}^{x} \sqrt{1 + \dot{f}(x)^2} dx, \tag{4}$$

where (x_0, y_0) is the start point of the path.

The heading angle of tangential direction $\theta(S)$ is defined by

$$\theta(S) = \arctan \dot{f}(x). \tag{5}$$

Based on (3), (4) and (5), the affine transformation between the two coordinates is obtained by

$$\begin{cases} \forall (x, y) \in \Omega_{x,y} \\ \exists : (x, y) \to S(x) \in \Omega_S, \theta(S) \in \Omega_\theta, \end{cases} \tag{6}$$

where $\Omega_{x,y} \in \mathbb{R}^2$ denotes the full point-set of the given path, $\Omega_S \in \mathbb{R}$ and $\Omega_\theta \in [0, 2\pi]$ denote the arc length-set and the tangential angle-set of the path, respectively.

According to (6), the moving road coordinate system ($\vec{s} \perp \vec{d}$) can be constructed and attached to the points of the given path. For example, there is a known point $\boldsymbol{O}$ with (X_o, Y_o) described in global coordinate system in Fig. 1. The transformation process of point $\boldsymbol{O}$ from X-Y to s-d coordinate is shown as

$$\begin{cases} s_o = S(x_A, y_A) \\ d_o = |\overrightarrow{AO}| \\ (x_A, y_A) \in \Omega_{x,y} \\ S(x_A, y_A) \in \Omega_S, \end{cases} \tag{7}$$

where point $\boldsymbol{A}$ is a point of the given path with the shortest distance to point $\boldsymbol{O}$, (x_A, y_A) is the global coordinate of point $\boldsymbol{A}$, (s_o, d_o) denotes the transformed s-d coordinate of point $\boldsymbol{O}$.

2) MOVING S-D TO X-Y COORDINATE

The information described in a moving coordinate system may require to be transformed into that of the global coordinate system for more convenient comparison and analysis. For example, Fig. 1 shows that based on the given road coordinate (s_o, d_o) of point $\boldsymbol{O}$, the inverse transformation is

$$\begin{cases} X_o = x_A + sign(\theta_A - \pi) d_o \sin\theta_A \\ Y_o = y_A + sign(\pi - \theta_A) d_o \cos\theta_A \\ s_o \to (x_A, y_A) \in \Omega_{x,y} \\ s_o \to \theta_A \in \Omega_\theta, \end{cases} \tag{8}$$

where θ_A is the angle between the moving s-d coordinate system fixed in point $\boldsymbol{A}$ and the global X-Y coordinate system.

C. ADAPTIVE POTENTIAL FIELD DEFINED IN ROAD COORDINATE SYSTEM

The PF defined in the global coordinate system may not adaptive to the curve road scenarios because of the different relative distances ($\Delta s \geq \Delta X$; $\Delta d \leq \Delta Y$). For the general application, the PF functions are defined under the road coordinate system in this paper.

The PF function of target lane is defined as

$$U_{TargL}(s, d) = a \left(d - d_{TrgL}\right)^2, \tag{9}$$

where d and d_{TrgL} denote the lateral distances of ego vehicle and target lane, and a is a shaping parameter.

The PF function of road boundary is defined as

$$U_{RBd}(s, d) = \begin{cases} b\,(d - d_{Br})^2 & d \leq d_{Br} \\ b\,(d_{Bl} - d)^2 & d \geq d_{Bl} \\ 0 & d \in (d_{Br}, d_{Bl}), \end{cases} \tag{10}$$

where b is a shaping parameter, d_{Bl} and d_{Br} denote the lateral positions of left and right road boundaries, respectively.

The obstacle PF (OPF) is designed to ensure the ego vehicle to keep a safe distance to the obstacle. The constructed OPF will guide the ego vehicle to take a lane-change or braking for safety while approaching to the obstacle. Based on the two-dimensional joint probability density distribution function (2D-PDF), the OPF can be defined as

$$N(\ell|\mu, \Sigma) = \frac{a_{obs}}{2\pi\sqrt{|\Sigma|}} e^{\left(-\frac{1}{2}(\ell-\mu)^T \Sigma^{-1} (\ell-\mu)\right)}, \tag{11}$$

where N is a 2D-PDF, a_{obs} is a comprehensive coefficient affected by the shape and type of the obstacle, $\ell = (s, d)^T$ is the position of ego vehicle in the road coordinate system, μ and Σ denote the mean and covariance matrix of the 2D-PDF, respectively.

Based on (11), the ADPF is designed to adaptive the acceleration/deceleration of the obstacles as

$$U_{ADPF} = w_1 N_1(\ell|\mu_1, \Sigma_1) + w_2 N_2(\ell|\mu_2, \Sigma_2), \tag{12}$$

where

$$w_1 \in [0.5, 1], \qquad w_1 + w_2 = 1,$$

$$\mu_1 = (s_1, d_1)^T, \quad \Sigma_1 = \begin{bmatrix} \sigma_{s_1}^2 & 0 \\ 0 & \sigma_{d_1}^2 \end{bmatrix},$$

$$\mu_2 = (s_2, d_2)^T, \quad \Sigma_2 = \begin{bmatrix} \sigma_{s_2}^2 & 0 \\ 0 & \sigma_{d_2}^2 \end{bmatrix},$$

N_1 and N_2 are two independent 2D-PDFs, U_{ADPF} is the adaptive potential field of obstacle, w_1 and w_2 denote the weights of two 2D-PDFs, μ_i and Σ_i $(i = 1, 2)$ are the mean and covariance matrix of the corresponding 2D-PDF, σ_{s_j} and σ_{d_j} $(j = 1, 2)$ denote the variance terms of the corresponding covariance matrix, respectively.

The definitions of the mean and covariance corresponding to N_1 are designed as

$$\begin{cases} s_1 = s_o,\ d_1 = d_o \\ \sigma_{s_1} = S_s - \Delta s \\ \sigma_{d_1} = S_d - \Delta d, \end{cases} \tag{13}$$

where (s_o, d_o) is the position of obstacle in road coordinate system, S_s and S_d denote the safe distances along the two directions of road coordinate system, Δs and Δd represent the biases relative to the obstacle position in two directions, respectively.

The corresponding mean and covariance of N_2 are defined as

$$\begin{cases} s_2 = s_o + \text{sign}(a_{s_o})\Delta s \\ d_2 = d_o + \text{sign}(a_{d_o})\Delta d \\ \sigma_{s_2} = S_s, \quad \sigma_{d_2} = S_d, \end{cases} \tag{14}$$

where $a_{s_o}(m/s^2)$ and $a_{d_o}(m/s^2)$ denote the longitudinal and lateral accelerations of the obstacle along road coordinate system, respectively.

The safe distance [23] is defined and calculated as

$$\begin{cases} S_s = S_0 + uT_0 + \dfrac{\Delta v_s^2}{2a_n} \\ S_d = D_0 + \dfrac{\Delta v_d^2}{2a_n}, \end{cases} \tag{15}$$

where S_0 and D_0 denote the minimum longitudinal and lateral distance decided by the geometric shape, T_0 is the safe time gap, Δv_s and Δv_d are the approaching velocities along the longitudinal and lateral directions of the road coordinate system, respectively; a_n is a tunable acceleration for optimizing the comfortable of ego vehicle, u is the velocity of ego vehicle.

The bias function is defined by

$$\begin{cases} \Delta q = \dfrac{S_{b,q}}{e^{-k(|a_q| - 0.5a_{q,max})}}, \quad (q = s, d), \\ S_{b,q} = k_q S_q \end{cases} \tag{16}$$

where $S_{b,q}$ denotes the tunable maximum bias along each direction of the road coordinate system, $a_{q,max}$ (m/s^2) denotes the maximum acceleration/deceleration of obstacle in each direction, k is a positive comprehensive coefficient.

Meanwhile, considering the mass of obstacle will influence the ADPF, i.e. the ADPFs of a car and a big box with the same accelerations should be different. The coefficient k_q is defined as

$$k_q = \begin{cases} 0 & m \in [0, 100) \\ e^{0.3\left(\frac{m}{1000} - 5\right)} & m \in [100, 5000) \\ 1 & m \in [5000, 12000), \end{cases} \tag{17}$$

where $m\,(kg)$ is the mass of obstacle, which is limited to under 12 tonnes [24] according to the vehicle categories of M_i and N_i, $i = 1, 2, 3$.

Table 1 demonstrates the related parameters for determining the ADPF. For example, considering the general driving situations, the longitudinal and lateral accelerations are limited in $[-0.3g, 0.3g]$ [25], respectively. The ADPFs with different accelerations/decelerations for the obstacle vehicle are shown in Fig. 2. The ⑤ in Fig. 2 shows that the OPF is symmetric when the longitudinal and lateral accelerations are equal to 0. The ④ and ⑥ of Fig. 2 show that the OPFs are asymmetric in the longitudinal direction when the obstacle vehicle is accelerating/decelerating along the longitudinal direction. Namely, the OPF values of its rear side is higher/lower than its front side in deceleration/acceleration scenarios, respectively. The OPFs are also asymmetric in the lateral direction when the lateral acceleration/deceleration happens (② and ⑧ in Fig. 2). For example, the OPF value to the left is obviously higher than that of the right side when the obstacle vehicle turning left. Meanwhile, subject to the nonholonomic constraints of the plane motion, the obstacle vehicle usually has both the longitudinal and lateral acceleration/deceleration while turning or changing lane, etc. The ADPFs in these longitudinal and lateral coupling situations are also shown in Fig. 2 (accelerating and steering: ③ and ⑨; decelerating and steering: ① and ⑦), which illustrate OPF values are asymmetrically distributed both in the longitudinal and lateral directions.

TABLE 1. Parameters of ADPF.

Parameter	Value	Parameter	Value	Parameter	Value
a_{obs}	$1e^4$	d_{TrgL}	1.75 m	a_q	$[-0.3g, 0.3g]$
w_1	0.7	d_{Bl}	6 m	$a_{q,max}$	$0.3g$
k	0.5	d_{Br}	1 m	b	100
g	9.8 (m/s^2)	a	0.5	(s_o, d_o)	$(50, 3)$

The mass of moving obstacle determines its inertia, which can be used to indicate the difficulty of state-changing. Since the difficulty of state-changing can be equivalent to the that of the collision-avoidance, the working range of the ADPF should be adaptive to the mass varying of the moving obstacle. Although the mass of obstacle vehicle cannot be detected by the on-board sensors, it can be estimated by the techniques of vehicle type recognition and classification. Fig. 3 shows the ADPFs of different obstacle vehicles with the same accelerations ($a_{s_o} = -0.3g, a_{d_o} = 0$). Fig. 3 indicates that the working range of ADPF will be enlarged with the vehicle's mass increase (Truck>Pickup>Car). Furthermore, the asymmetric feature of ADPF is more obvious when the mass is larger.

III. AN ADAPTIVE POTENTIAL FIELD BASED PATH PLANNING

The path planning and tracking for AVs can be solved separately as a hierarchical framework with two independent parts or integrated as an entire part. In a hierarchical

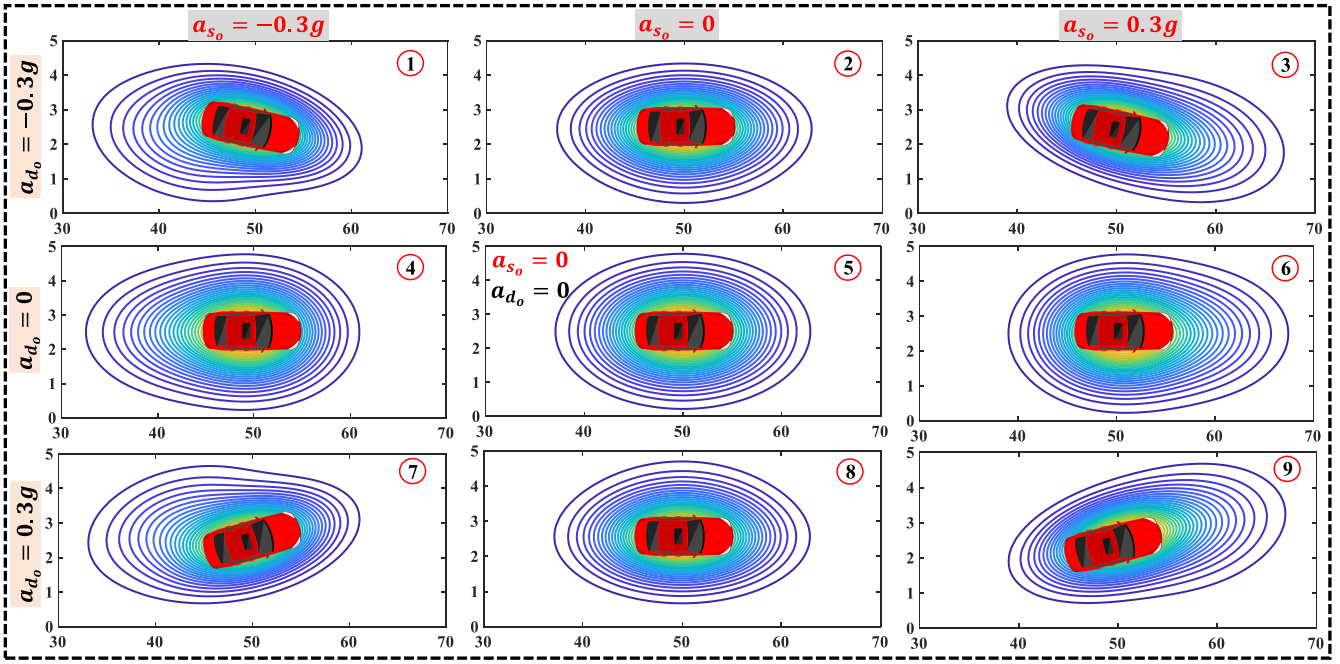

FIGURE 2. ADPFs with different longitudinal and lateral accelerations: $(a_{s_o}, a_{d_o}) \in [-0.3g, 0.3g]$.

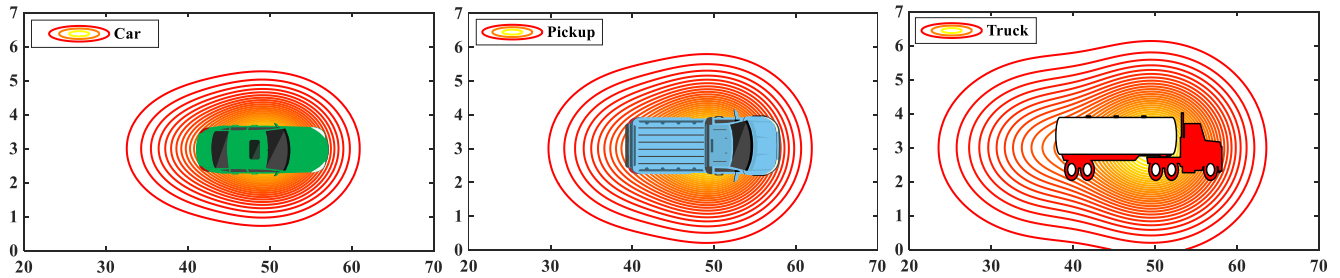

(a) Car: $m = 2000kg$ (b) Pickup: $m = 4500kg$ (c) Truck: $m = 8000kg$

FIGURE 3. ADPFs of different vehicles with the same accelerations: $a_{s_o} = -0.3g, a_{d_o} = 0$.

framework, a reference path is planned firstly, then a controller is designed to track the planned path [26], [27]. The integrated solution method aims to improve the time delay of tracking by directly outputting the reference control variables rather than the expected reference route [28]. Considering the computation cost and simplicity for validation, the hierarchical framework is applied for the path planning and tracking based on the ADPF in this paper.

A. THE ADPF ESTABLISHING

The potential field-based path planning is likely to be trapped into local minima, especially in an unknown environment [29]. To avoid the local optima problem in the proposed path planning method, both the driving environment and the obstacles (vehicles) are assumed to be known, thus we can design and establish the potential fields more appropriately. Besides, we design the attractive potential field with the center line of the target lane to attract the ego vehicle driving to the target lane instead of with only one target point, which will reduce the chance to trap into the local optima by solving a series of optimization subproblems.

1) THE ACCELERATION/DECELERATION ESTIMATION OF MOVING OBSTACLE

The longitudinal and lateral accelerations of ego vehicle (a_x, a_y) in the global coordinate system can be obtained with the on-board sensors (GNSS/INS). Meanwhile, based on the other on-board sensors (camera/radar/lidar), the relative accelerations/decelerations $(\Delta a_{s_e}, \Delta a_{d_e})$ between the ego vehicle and the moving obstacle can be calculated in the road coordinate system. To achieve the acceleration of moving obstacle in the road coordinate system (a_{s_o}, a_{d_o}), a rotation in the road coordinate system ($\vec{s}_e \perp \vec{d}_e$ and $\vec{s}_o \perp \vec{d}_o$) is required.

Fig. 4 shows that (s_e, d_e, θ_e) and (s_o, d_o, θ_o) are the position descriptions of the ego vehicle and obstacle vehicle in the

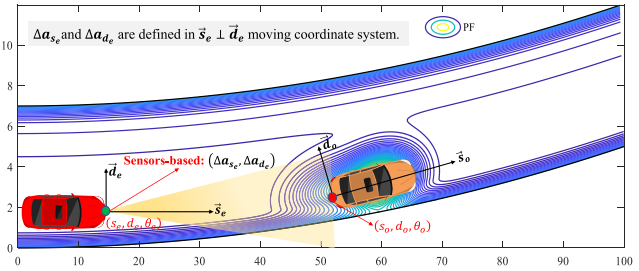

FIGURE 4. The acceleration/deceleration detection of moving obstacles.

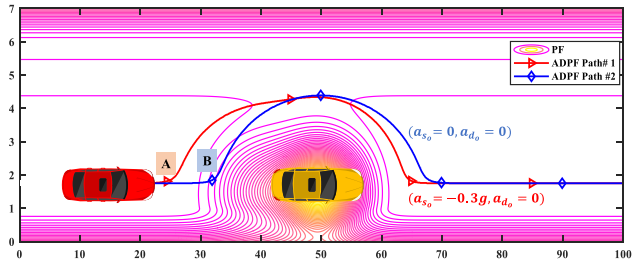

FIGURE 5. The planned paths of ADPF-PP with different decelerations of the obstacle vehicle on straight roads.

moving road coordinate system, respectively. $\vec{s}_e \perp \vec{d}_e$ and $\vec{s}_o \perp \vec{d}_o$ denote the corresponding moving coordinates of ego vehicle and obstacle vehicle, respectively.

The rotation matrix is defined as

$$\boldsymbol{M}(\theta) = \begin{bmatrix} \cos\theta & -\sin\theta \\ \sin\theta & \cos\theta \end{bmatrix}, \tag{18}$$

where θ (rad) is the angle between two coordinate systems.

The accelerations/decelerations of ego vehicle (a_{s_e}, a_{d_e}) in corresponding road coordinate system is calculated as

$$\begin{bmatrix} a_{s_e} \\ a_{d_e} \end{bmatrix} = \boldsymbol{M}(\theta_e) \begin{bmatrix} a_x \\ a_y \end{bmatrix}, \tag{19}$$

where a_x and a_y denote the longitudinal and lateral accelerations of ego vehicle in the global X-Y coordinate system, θ_e (tangential angle of the road) is the angle between the road coordinate system of ego vehicle and the X-Y coordinate system, a_{s_e} and a_{d_e} are the tangential and perpendicular accelerations of ego vehicle in corresponding road coordinate system, respectively.

The accelerations/decelerations of obstacle (a_{s_o}, a_{d_o}) in corresponding road coordinate system are estimated as

$$\begin{bmatrix} \Delta a_{s_e} \\ \Delta a_{d_e} \end{bmatrix} = \begin{bmatrix} a_{s_e} \\ a_{d_e} \end{bmatrix} - \boldsymbol{M}(\theta_o - \theta_e) \begin{bmatrix} a_{s_o} \\ a_{d_o} \end{bmatrix}, \tag{20}$$

where θ_o is the angle between the road coordinate system of obstacle vehicle and the global coordinate system, a_{s_o} and a_{d_o} are the tangential and normal accelerations in corresponding $\vec{s}_o \perp \vec{d}_o$ road coordinate system, Δa_{s_e} and Δa_{d_e} are the relative accelerations between ego vehicle and obstacle vehicle calculated in the road coordinate system of ego vehicle.

B. PATH GENERATION WITH ADPF

The PFs are updated in real-time with the position and acceleration/deceleration of moving obstacle during path planning. Meanwhile, the ADPF-PP generates the collision-free path with the minimum PF by solving

$$\min_{(s_{min}, d_{min})} \left\{ U_{TargL} + U_{RBd} + U_{ADPF} \right\}, \tag{21}$$

where (s_{min}, d_{min}) denotes the point-set of planned path.

As shown in Fig. 5, the planned paths of ADPF-PP vary with the obstacle vehicle's decelerations. The planned paths are highlighted in red and blue when the decelerations of the obstacle vehicle are $(a_{s_o} = -0.3g, a_{d_o} = 0)$ and $(a_{s_o} = 0, a_{d_o} = 0)$, respectively. The generated paths show that the ego vehicle will take a lane-change to avoid the yellow obstacle vehicle. However, the lane-change points are different in the two trajectories (point A *vs* point B), which indicates that the different braking severity of the obstacle vehicle will result in different driving maneuvers of the following vehicle.

In a lane change or a cut-in driving scenario of the obstacle vehicle, both acceleration and steering maneuvers would frequently occur [30]. Thus, the ego vehicle would take different responses (e.g., braking, steering, and lane keeping) according to the velocity and acceleration of the obstacle vehicle. Fig. 6 shows the cut-in of the obstacle vehicle with different accelerations while driving on curve roads. Both of the two routes will lead the ego vehicle to depart the target path for safety when the obstacle vehicle is laterally approaching from the left lane. However, the departure moment is different between the examined situations, indicating that the driving maneuver of the ego vehicle depends on the acceleration and steering aggressiveness of the obstacle vehicle. The illustrated blue trajectory will result in an earlier departure of the ego vehicle than that of the red one (point A *vs* point B), which indicates that a smaller acceleration of the obstacle vehicle should correspond to an earlier lane departure behavior for driving safety.

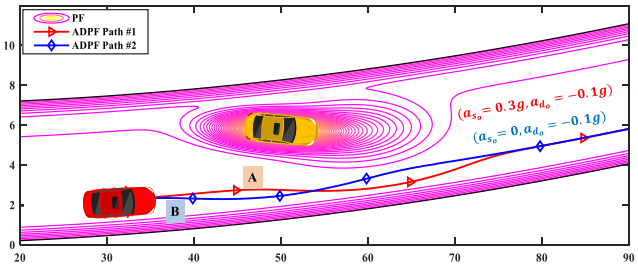

FIGURE 6. The planned paths of ADPF-PP for cut-in with different accelerations of the obstacle vehicle on curve roads.

Therefore, as illustrated in the trajectories in Fig. 5 and Fig. 6, our proposed ADPF-PP can adaptively adjust the moments of lane change and lane departure according to the different behaviors of the obstacle vehicle.

IV. SIMULATION AND DISCUSSION

A. COMPLEX DRIVING SCENARIOS FOR SIMULATIONS

1) CUT-IN AND DECELERATING DRIVING SCENARIO

A cut-in and decelerating scenario is established in the straight road environment in Fig. 7. The blue vehicle as a

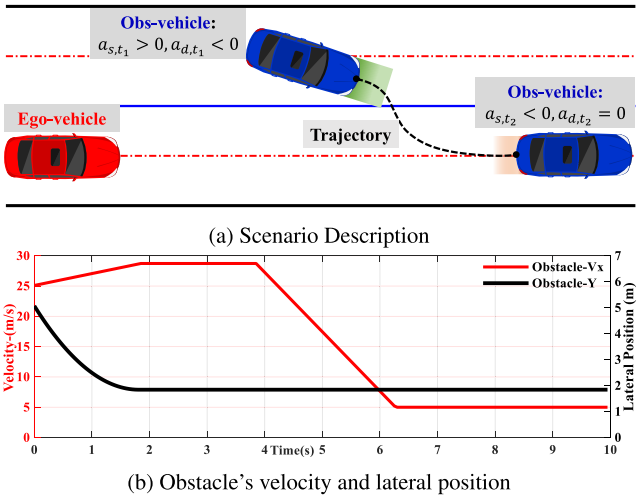

FIGURE 7. Driving scenario A for simulation: cut-in & emergency decelerating.

moving obstacle will cut into the target lane at the time of t_1, furthermore, the blue vehicle will take an emergency decelerating at the time of t_2 after the lane change as Fig. 7a shown. The relevant states are presented in Fig. 7b, which the red and black solid lines denote the speed and lateral position of the blue vehicle. It illustrates that the blue vehicle will accelerate to cut into the target lane from time of 0s to 2s and decelerate to 5 m/s with a deceleration of $-0.8g$ after the time of 3.8s.

2) OVERTAKING WITH OBSTACLE ACCELERATING DRIVING SCENARIO

The velocity and acceleration of the front car are essential for the ego vehicle to make a decision of lane change or lane keeping in practical driving scenarios as shown in Fig. 8a. A complex driving scenario is designed to reveal this phenomenon, i.e. the ego vehicle need to decide whether to take

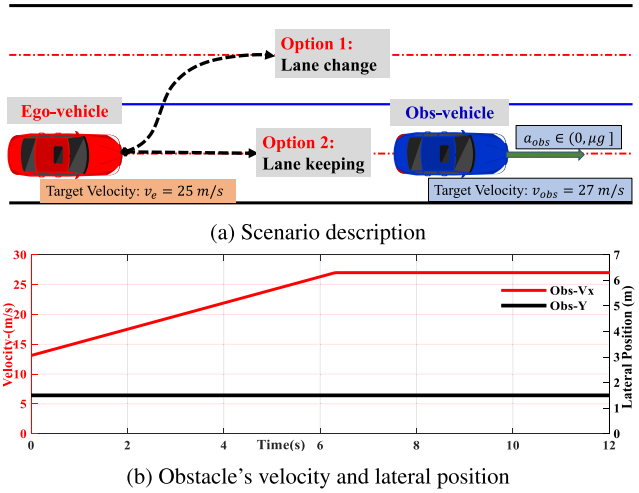

FIGURE 8. Driving scenario B for simulation: The obstacle is accelerating during overtaking.

an overtaking when the front car is accelerating. The velocity and lateral position of the blue car are shown in Fig. 8b, which denotes that the initial and final velocities are set to 14 m/s and 27 m/s, respectively. Meanwhile, the blue car is accelerating to the final velocity with a 2 m/s^2 acceleration at the beginning.

3) CURVE ROAD DRIVING SCENARIO

The ADPF-PP should be adaptive to both the straight road and curve road scenario. To examine the robustness of ADPF-PP, a curve road scenario is designed in Fig. 9. There are three vehicles in the curve road driving scenario, i.e. a green passenger car, a light blue pickup and a red truck, are used as the obstacles in front of the red ego vehicle on the target lane. The speeds of the obstacles (5 m/s) are smaller than the target speed of the ego vehicle.

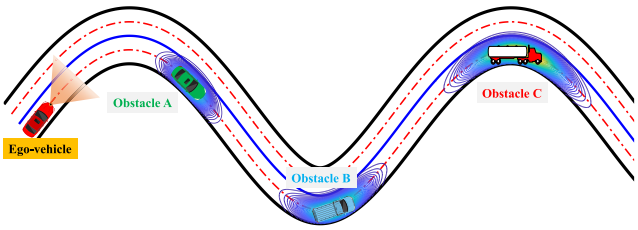

FIGURE 9. Driving scenario C for simulation: Curve road environment.

4) AN ACTIVE LANE CHANGE SCENARIO WITH REAL DATA

A crowd highway driving scenario with real information of surrounding vehicles is extracted from the highD dataset to further examine the effectiveness of the proposed method. The scenario is shown in Fig. 10a. Four obstacle vehicles are driving in Lane #1 and Lane #3, and the ego vehicle needs to take a lane change from the current lane to the target lane (Lane #3) because of a slow driving truck far ahead which is not illustrated in Fig. 10a. The far distance with the lead slow truck allows the ego vehicle to move laterally to the left lane when it is safe instead of to take a dangerous sudden lane change. The speed profiles of the four obstacle vehicles are shown in Fig. 10b.

B. MPC-BASED PATH TRACKING

The MPC controller is used as a path tracking module. To balance the computation cost and the model accuracy, the 3-DOF vehicle dynamics model in Fig.11 is used as the prediction model.

The formulations for 3-DOF dynamics model [31] are presented as

$$\begin{cases} m\left(\dot{v}_x - \omega v_y\right) = F_x \cos\delta \\ m\left(\dot{v}_y + \omega v_x\right) = F_{y,r} + F_{y,f}\cos\delta \\ I_z\dot{\omega} = F_{y,f}L_f\cos\delta - F_{y,r}L_r. \end{cases} \tag{22}$$

The motion formulations of the vehicle are shown as

$$\begin{cases} \dot{X} = v_x\cos\varphi - v_y\sin\varphi \\ \dot{Y} = v_x\sin\varphi + v_y\cos\varphi, \end{cases} \tag{23}$$

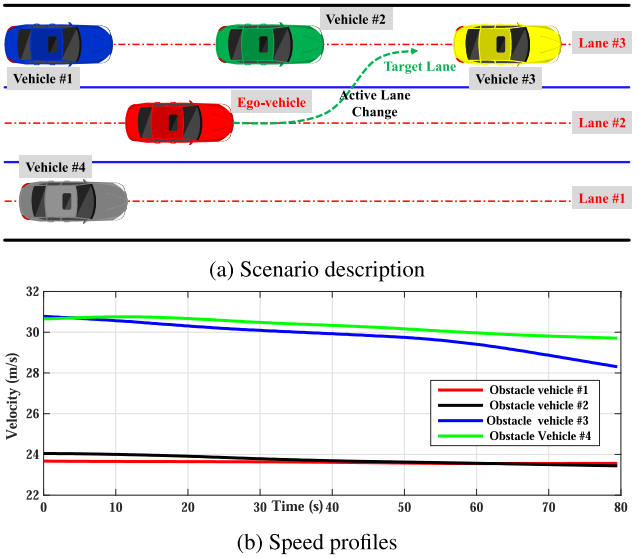

FIGURE 10. Driving scenario D: A scenario with real data based on highD dataset.

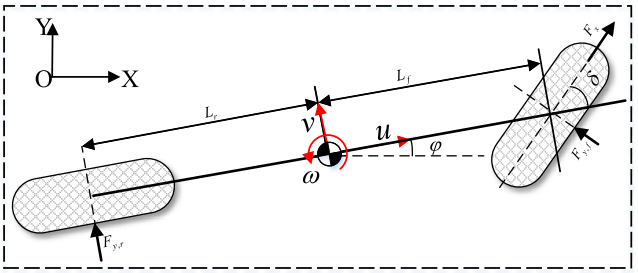

FIGURE 11. The 3-DOF vehicle dynamics model.

where v_x, v_y and ω are the longitudinal, lateral velocity and yaw rate of the vehicle, respectively. X, Y and φ denote the longitudinal and lateral positions, and the heading angle, m and F_x represent the vehicle mass and longitudinal force of the front-driving tire based on the linear tire model [32], $F_{y,f}$ and $F_{y,r}$ denote the lateral force of front and rear tires, L_f, L_r and I_z represent the front and rear wheelbases, and the vehicle inertia around vertical axis.

Based on the optimal control theory, a quadratic cost function is designed for MPC tracking control. The optimization problem can be described as follows:

$$\begin{aligned}
&\min_{\Delta U_t} \sum_{k=1}^{N_p} \|y_{t+k,t} - y^{des}_{t+k,t}\|^2_{\mathbf{Q}} + \|\Delta u_{t+k-1,t}\|^2_{\mathbf{R}} \\
&s.t.\ (k = t, .., t + N_p - 1) \\
&\quad x_t^{k+1} = \mathbf{A}_d x_t^k + \mathbf{B}_d u_t^k \\
&\quad y_{k,t} = \mathbf{C}_d x_t^k \\
&\quad y_{min} \le y_{k,t} \le y_{max} \\
&\quad u_{min} \le u_{k,t} \le u_{max} \\
&\quad \Delta u_{k,t} \in [\Delta u_{min}, \Delta u_{max}] \\
&\quad u_{k,t} = u_{k-1,t} + \Delta u_{k,t}
\end{aligned} \tag{24}$$

where $\mathbf{Q}$ and $\mathbf{R}$ are the weights of the cost terms, k represents the prediction of k^{th} step ahead of t; $\mathbf{A}_d$ and $\mathbf{B}_d$ are the discrete matrices of the state-equation based on Euler method [33]; $\mathbf{C}_d$ denotes the output matrix, $y^{des}_{t+k,t}$ represents the reference path generated by ADPF-PP; $y_{t+k,t}$ is the real-time position of the ego vehicle. The Optimal problem is solved by an open-source solver qpOASES [34]. The basic parameters of the vehicle model are in the Table 1 of [32]. The relative parameters of the MPC controller are described and configured in Table 2.

TABLE 2. Parameters for MPC controller.

Symbol	Description	Value [units]
N_p	Prediction Horizon	20 [-]
N_u	Control Variables Number	2 [-]
N_s	State Variables Number	6 [-]
T_s	Sampling Period	0.05 $[s]$
δ_w	Limitation of Steering Wheel Angle	$[-540, 540]$ $[^\circ]$
$\Delta\delta_w$	Steering Wheel Angle Rate	$[-5, 5]$ $[^\circ]$
F_x	Longitudinal Tire Force Limitation	$[-2000, 2000]$ $[N]$
ΔF_x	Tire Force Rate Limitation	$[-50, 50]$ $[N]$
$\boldsymbol{Q}$	Weights for Reference Tracking	$diag(1e^{-7}\ 1e^{2}\ 1e^{-4}\ 0\ 0\ 0)$
$\boldsymbol{R}$	Weights for Control Variables	$diag(1e^{-7}\ 5e^{-3})$

C. RESULTS AND DISCUSSIONS

An improved potential field-based path planning (IPF-PP) method [35] and the classical CPF-PP method are used for comparison with the proposed approach in this study. The results are presented as follows.

The initialization parameters of scenario A are shown in Table 3. The initial and target velocities of the ego vehicle are set as 25 m/s. The corresponding results in scenario A are shown in Fig. 12, where the lateral positions and the speeds of the ego vehicle when using different methods are compared in 12a and Fig. 12b, respectively. The lateral position results indicate that these methods are sensitive to the lateral approaching of the obstacle, because the lane departures happen during the lateral approaching process ($0s \sim 2s$) of the obstacle. Differently, the planned path of ADPF will guide the ego vehicle to take a lane change earlier than the two compared methods for better driving safety performance during the emergency braking of the lead car from 3.8 s to 6.2 s. The comparison of tracking velocities indicates that the driving efficiencies of these approaches are almost the same. These results show that the proposed ADPF can improve the driving safety without decreasing the driving efficiency.

TABLE 3. Initialization parameters of scenario A.

Ego vehicle	Configuration	Obstacle vehicle	Configuration
Initial position	$(0\ m, 1.75\ m)$	Initial position	$(10\ m, 5.25\ m)$
Initial velocity	$25\ m/s$	Initial velocity	$25\ m/s$
Target velocity	$25\ m/s$	Final velocity	$5\ m/s$
Target lane	$\#\ 1$	Target lane	$\#\ 1$

The quantitative indexes shown in Table 4 (i.e., ω_{max}, $\bar{V}_x$, $a_{y,max}$ and TTC) are used to evaluate the performance of the

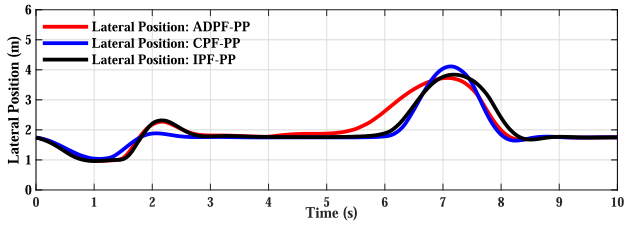

(a) Lateral positions: ADPF-PP, CPF-PP and IPF-PP

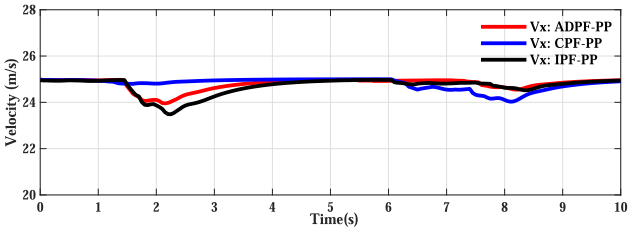

(b) Tracking velocities: ADP-PPF, CPF-PP and IPF-PP

FIGURE 12. The results comparison of scenario A.

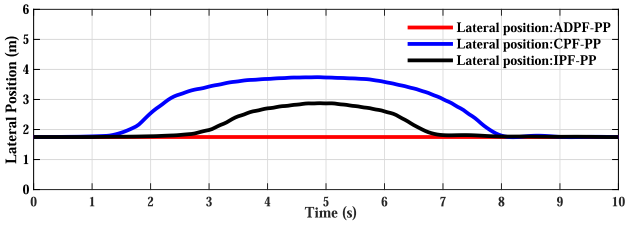

(a) Lateral positions: ADPF-PP, CPF-PP and IPF-PP

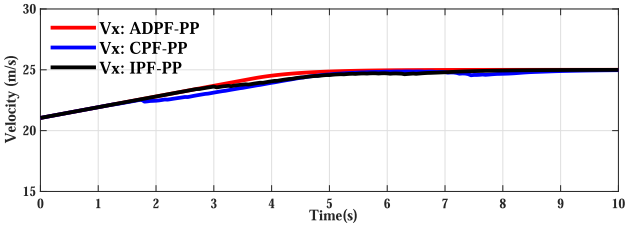

(b) Tracking velocities: ADPF-PP, CPF-PP and IPF-PP

FIGURE 13. The results comparisons of the driving scenario B.

TABLE 4. Results of different methods in scenario A.

Item	Description	ADPF-PP	CPF-PP	IPF-PP
ω_{max} (deg/s)	Maximum yaw rate	18.37	44.69	29.95
$\bar{V}_x$ (m/s)	Average passing velocity	24.772	24.774	24.708
$a_{y,max}$ (m/s^2)	Maximum lateral acceleration	4.4	7.9	6.02
TTC (s)	Time-to-Collision of LC point	4.9	1.3	2.02

examined methods from different aspects including vehicle stability, driving comfort, and driving safety. The detailed descriptions of these indexes are given in Table 4, as well as the corresponding results when using different methods. The comparison results on ω_{max} show that the proposed ADPF-PP method can achieve a better vehicle stability performance than the other two compared methods. The $\bar{V}_x$ is almost the same across these three compared methods. The lowest $a_{y,max}$ when using ADPF-PP shows the superiority to the other two methods on driving comfort, and the TTC results show that the driving safety with ADPF-PP can be effectively improved with almost the same passing velocities.

The initialization parameters of scenario B are shown in Table 5 including the velocities and positions of the ego vehicle and the obstacle vehicle, respectively. The comparison results when using different methods in scenario B are shown in Fig. 13. The comparison of the lateral positions shows that the generated paths of CPF-PP and IPF-PP lead the ego vehicle to take a lane change for overtaking when the lead vehicle is accelerating. However, this is not reasonable

TABLE 5. Initialization parameters of scenario B.

Ego vehicle	Configuration	Obstacle vehicle	Configuration
Initial position	(0 m, 1.7 m)	Initial position	(15 m, 1.7 m)
Initial velocity	20 m/s	Initial velocity	14 m/s
Target velocity	25 m/s	Final velocity	27 m/s
Acceleration	/	Acceleration	2 m/s^2

because the speed of the lead vehicle is already higher than the target velocity of the ego vehicle before the time of 8 s (27 m/s *vs* 25 m/s), thus the lane change is not needed for safety reasons but may result in worse driving comfort and increase the risk of sideswipe crashes. The tracking velocity results show that the driving efficiency when using different methods are almost the same.

The quantitative results when using different methods are shown in Table 6. Similar with the results shown in Table 4, the comparison results on all the examined indexes show the same trends as in scenario A. The ego vehicle with ADPF-PP will only take a lane change when the acceleration of the front vehicle is less than 2.2 m/s^2, which is smaller than that of the CPF-PP (3.5 m/s^2) and the IPF-PP (3 m/s^2). Since the ADPF-PP has a lower acceleration threshold, it can efficiently decrease the unnecessary lane changes to improve the driving safety and driving comfort of autonomous vehicles.

TABLE 6. Results of different methods in scenario B.

Item	Description	ADPF-PP	CPF-PP	IPF-PP
ω_{max} (deg/s)	Maximum yaw rate	0	25.15	17.85
$a_{y,max}$ (m/s^2)	Maximum lateral acceleration	0	4.5	3.5
$\bar{V}_x$ (m/s)	Average passing velocity	24.35	24.19	24.25
a_{LC} (m/s^2)	Acceleration threshold without LC	≥ 2.2	≥ 3.5	≥ 3

Since the PFs of IPF-PP and CPF-PP are designed under the Cartesian coordinate system, they cannot be used in a curve road scenario for comparisons. Therefore, the driving scenario C is only used to verify the feasibility and robustness of ADPF-PP. The initial and target velocities of the ego vehicle are set to 15 m/s and 20 m/s, respectively. The results when using ADPF-PP in driving scenario C are shown in Fig. 14. The results of tracking velocity and the steering command show that the velocity can be well tracked with ADPF-PP in the curve road scenario, and the planned path (red route in Fig. 14b) of ADPF-PP shows that ADPF

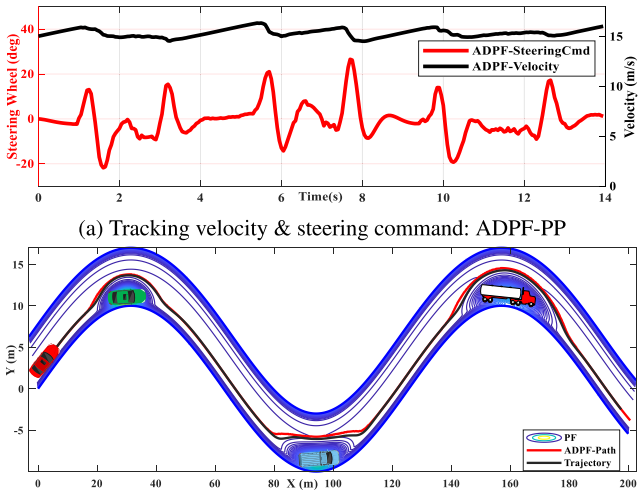

(a) Tracking velocity & steering command: ADPF-PP

(b) Path planning & tracking: ADPF-PP

FIGURE 14. The results of ADPF-PP in scenario C.

is automatically adaptive to the mass of obstacle vehicles. Furthermore, the black trajectory shows that the planned path can be well tracked. These results support that the proposed path planning approach can be well applied in the curve road environments. The quantitative results when using ADPF-PP in scenario C are shown in Table 7. The examined indexes of ω_{max}, $a_{y,max}$ and $\bar{V}_x$ show that the ego vehicle with ADPF-PP can avoid the obstacles with a good vehicle stability, ride comfort and driving efficiency in a curve road environment.

TABLE 7. Results of ADPF-PP in scenario C.

Item	Description	ADPF-PP
ω_{max} (deg/s)	Maximum yaw rate	32.15
$a_{y,max}$ (m/s^2)	Maximum lateral acceleration	3.2
$\bar{V}_x$ (m/s)	Average passing velocity	15.36

The extracted parameters from a crowd highway driving scenario in the naturalistic driving dataset highD are used to design scenario D, and parameter values are shown in Table 8. As illustrated in Figure 10, the ego vehicle intends to laterally move to the left lane. According to the extracted information, the target speed of the ego vehicle is set as 23 m/s and the target lane is set Lane #3.

The corresponding lateral position and tracking velocity results of the ego vehicle when using different methods are shown in Fig. 15. The lateral position results indicate that the ego vehicle will not take a lane change immediately because of the current crowd and unsafe situation in the target lane. The ego vehicle will only take a lane change maneuver when there is a safe distance gap for lane change in the target lane. Fig. 15a shows that the moment of lane change when using ADPF-PP is later than the moments when using the other two methods, because both the velocities and accelerations of the obstacles are considered to establish the potential field for safety improvement in ADPF-PP. Similarly, the velocities of

TABLE 8. Initialization parameters of scenario D.

Vehicle number	Initial X (m)	Initial Y (m)	Initial velocity (m/s)	Lane
Vehicle #1	185	8.8	23.67	#3
Vehicle #2	249	8.65	24.05	#3
Vehicle #3	287	1.5	30.76	#1
Vehicle #4	401	8.6	30.65	#3
Ego vehicle	190	5.25	24	#2

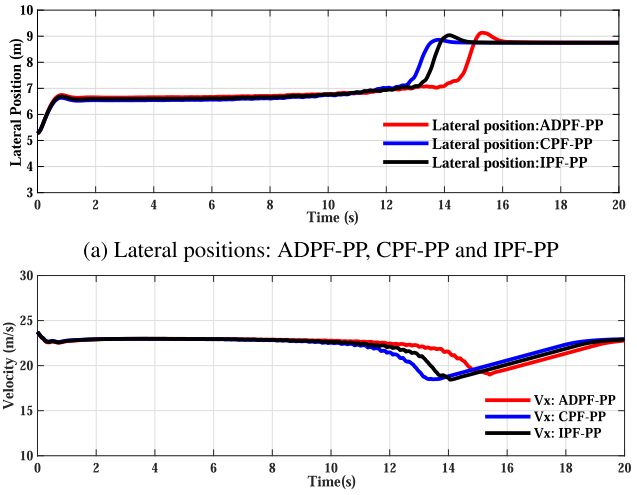

(a) Lateral positions: ADPF-PP, CPF-PP and IPF-PP

(b) Tracking velocities: ADPF-PP, CPF-PP and IPF-PP

FIGURE 15. A driving scenario with real data based on the highD dataset.

the ego vehicle shown in Fig. 15b indicate that the driving efficiencies when using different methods are also almost the same in scenario D.

The quantitative results when using different methods are shown in Table 9. The comparison results on the examined indexes of ω_{max}, $a_{y,max}$ and $\bar{V}_x$ show the same trends as in scenario A and scenario B. The comparison results of D_{safe} show that the driving safety with ADPF-PP can be effectively improved with a larger interval distance during lane change.

TABLE 9. Results of different methods in scenario D.

Item	Description	ADPF-PP	CPF-PP	IPF-PP
ω_{max} (deg/s)	Maximum yaw rate	73.07	79.05	77.43
$a_{y,max}$ (m/s^2)	Maximum lateral acceleration	5.42	5.63	5.57
$\bar{V}_x$ (m/s)	Average passing velocity	22.28	22.16	22.17
D_{safe} (m)	Interval distance of LC point	12.99	12.76	12.95

All the above results show that the proposed approach can be used to improve the driving safety and driving comfort while retaining the driving efficiency in various driving scenarios on both straight roads and curve roads.

V. CONCLUSION

The potential fields are redesigned to establish the PF of the obstacles by considering the mass and acceleration/deceleration of the obstacle in a transformed road coordinate system. A path planning based on the redesigned potential field (ADPF) is proposed to improve the driving safety and ride comfort of AVs in complex driving scenarios.

The complex driving scenarios, which including a cut-in and emergency braking scenario, an overtaking scenario with accelerating lead vehicle and a curve road driving scenario, are constructed to verify the effectiveness and robustness of the proposed approach. Furthermore, a driving scenario with real information of the environment vehicles is used to examine and to evaluate the method. The results in the cut-in and emergency braking scenarios illustrate that the ADPF-PP can improve the driving safety with almost 3 times improvement on *TTC* for obstacle avoidance, and the unnecessary lane change maneuvers can be efficiently decreased almost 37.14% in the overtaking scenario. The results of the curve road scenario verified the feasibility and robustness of the proposed algorithm to the curve road environment.

In our future work, more experiments on a vehicle-in-loop (VIL) platform or in on-road real driving scenarios should be further conducted for improvement and validation of the proposed method. Meanwhile, how the local optima problem can be completely or sufficiently avoided in more complex and unknown driving scenarios with more traffic participants is still a challenging task and should be further addressed in the future work to improve the robustness of the proposed methods.

ACKNOWLEDGMENT

The authors would like to thank the anonymous reviewers for their comments and suggestions.

REFERENCES

[1] L. Hu, W. Naeem, E. Rajabally, G. Watson, T. Mills, Z. Bhuiyan, C. Raeburn, I. Salter, and C. Pekcan, "A multiobjective optimization approach for COLREGs-compliant path planning of autonomous surface vehicles verified on networked bridge simulators," *IEEE Trans. Intell. Transp. Syst.*, vol. 21, no. 3, pp. 1167–1179, Mar. 2020.

[2] L. Claussmann, M. Revilloud, D. Gruyer, and S. Glaser, "A review of motion planning for highway autonomous driving," *IEEE Trans. Intell. Transp. Syst.*, vol. 57, no. 4, pp. 1826–1848, May 2019.

[3] Y. Zhang, H. Chen, S. L. Waslander, J. Gong, G. Xiong, T. Yang, and K. Liu, "Hybrid trajectory planning for autonomous driving in highly constrained environments," *IEEE Access*, vol. 6, pp. 32800–32819, Jun. 2018.

[4] L. Schmid, M. Pantic, R. Khanna, L. Ott, R. Siegwart, and J. Nieto, "An efficient sampling-based method for online informative path planning in unknown environments," *IEEE Robot. Autom. Lett.*, vol. 5, no. 2, pp. 1500–1507, Apr. 2020.

[5] R. Song, Y. Liu, and R. Bucknall, "Smoothed A* algorithm for practical unmanned surface vehicle path planning," *Appl. Ocean Res.*, vol. 83, pp. 9–20, Feb. 2019.

[6] T. T. Mac, C. Copot, D. T. Tran, and R. De Keyser, "Heuristic approaches in robot path planning: A survey," *Robot. Auto. Syst.*, vol. 86, pp. 13–28, Dec. 2016.

[7] W. Lim, S. Lee, M. Sunwoo, and K. Jo, "Hybrid trajectory planning for autonomous driving in on-road dynamic scenarios," *IEEE Trans. Intell. Transp. Syst.*, early access, Dec. 13, 2019, doi: 10.1109/TITS.2019.2957797.

[8] G. Li, Y. Yang, and X. Qu, "Deep learning approaches on pedestrian detection in hazy weather," *IEEE Trans. Ind. Electron.*, vol. 67, no. 10, pp. 8889–8899, Oct. 2020.

[9] H. Wang, Y. Huang, A. Khajepour, Y. Zhang, Y. Rasekhipour, and D. Cao, "Crash mitigation in motion planning for autonomous vehicles," *IEEE Trans. Intell. Transp. Syst.*, vol. 20, no. 9, pp. 3313–3323, Sep. 2019.

[10] B. Li, H. Du, and W. Li, "A potential field approach-based trajectory control for autonomous electric vehicles with in-wheel motors," *IEEE Trans. Intell. Transp. Syst.*, vol. 18, no. 8, pp. 2044–2055, Aug. 2017.

[11] S. M. H. Rostami, A. K. Sangaiah, J. Wang, and X. Liu, "Obstacle avoidance of mobile robots using modified artificial potential field algorithm," *EURASIP J. Wireless Commun. Netw.*, vol. 2019, no. 1, p. 70, Mar. 2019.

[12] A. H. Qureshi and Y. Ayaz, "Potential functions based sampling heuristic for optimal path planning," *Auto. Robots*, vol. 40, no. 6, pp. 1079–1093, Aug. 2016.

[13] Y.-B. Chen, G.-C. Luo, Y.-S. Mei, J.-Q. Yu, and X.-L. Su, "UAV path planning using artificial potential field method updated by optimal control theory," *Int. J. Syst. Sci.*, vol. 47, no. 6, pp. 1407–1420, Apr. 2016.

[14] Y. Huang, H. Ding, Y. Zhang, H. Wang, D. Cao, N. Xu, and C. Hu, "A motion planning and tracking framework for autonomous vehicles based on artificial potential field elaborated resistance network approach," *IEEE Trans. Ind. Electron.*, vol. 67, no. 2, pp. 1376–1386, Feb. 2020.

[15] Y. Rasekhipour, A. Khajepour, S.-K. Chen, and B. Litkouhi, "A potential field-based model predictive path-planning controller for autonomous road vehicles," *IEEE Trans. Intell. Transp. Syst.*, vol. 18, no. 5, pp. 1255–1267, May 2017.

[16] J. Wang, J. Wu, and Y. Li, "The driving safety field based on driver-vehicle-road interactions," *IEEE Trans. Intell. Transp. Syst.*, vol. 16, no. 4, pp. 2303–2314, Aug. 2015.

[17] J. Wang, J. Wu, X. Zheng, D. Ni, and K. Li, "Driving safety field theory modeling and its application in pre-collision warning system," *Transp. Res. Part C, Emerg. Technol.*, vol. 72, pp. 306–324, Nov. 2016.

[18] U. Orozco-Rosas, K. Picos, and O. Montiel, "Hybrid path planning algorithm based on membrane pseudo-bacterial potential field for autonomous mobile robots," *IEEE Access*, vol. 7, pp. 156787–156803, Oct. 2019.

[19] K. Jiang, D. Yang, S. Xie, Z. Xiao, A. C. Victorino, and A. Charara, "Real-time estimation and prediction of tire forces using digital map for driving risk assessment," *Transp. Res. Part C, Emerg. Technol.*, vol. 107, pp. 463–489, Oct. 2019.

[20] M.-Y. Yu, R. Vasudevan, and M. Johnson-Roberson, "Occlusion-aware risk assessment for autonomous driving in urban environments," *IEEE Robot. Autom. Lett.*, vol. 4, no. 2, pp. 2235–2241, Apr. 2019.

[21] R. Krajewski, J. Bock, L. Kloeker, and L. Eckstein, "The highD dataset: A drone dataset of naturalistic vehicle trajectories on German highways for validation of highly automated driving systems," in *Proc. 21st Int. Conf. Intell. Transp. Syst. (ITSC)*, Nov. 2018, pp. 2118–2125.

[22] H. Taghavifar, "Neural network autoregressive with exogenous input assisted multi-constraint nonlinear predictive control of autonomous vehicles," *IEEE Trans. Veh. Technol.*, vol. 68, no. 7, pp. 6293–6304, Jul. 2019.

[23] S. Magdici and M. Althoff, "Adaptive cruise control with safety guarantees for autonomous vehicles," *IFAC-PapersOnLine*, vol. 50, no. 1, pp. 5774–5781, Jul. 2017.

[24] T. Trost, M. Sterner, and T. Bruckner, "Impact of electric vehicles and synthetic gaseous fuels on final energy consumption and carbon dioxide emissions in Germany based on long-term vehicle fleet modelling," *Energy*, vol. 141, pp. 1215–1225, Dec. 2017.

[25] B. Gutjahr, L. Gröll, and M. Werling, "Lateral vehicle trajectory optimization using constrained linear time-varying MPC," *IEEE Trans. Intell. Transp. Syst.*, vol. 18, no. 6, pp. 1586–1595, Jun. 2017.

[26] C. Zhang, D. Chu, S. Liu, Z. Deng, C. Wu, and X. Su, "Trajectory planning and tracking for autonomous vehicle based on state lattice and model predictive control," *IEEE Intell. Transp. Syst. Mag.*, vol. 11, no. 2, pp. 29–40, Mar. 2019.

[27] A. Abadi, A. El Amraoui, H. Mekki, and N. Ramdani, "Optimal trajectory generation and robust flatness–based tracking control of quadrotors," *Optim. Control Appl. Methods*, vol. 40, no. 4, pp. 728–749, May 2019.

[28] C. Shen, Y. Shi, and B. Buckham, "Integrated path planning and tracking control of an AUV: A unified receding horizon optimization approach," *IEEE/ASME Trans. Mechatronics*, vol. 22, no. 3, pp. 1163–1173, Jun. 2017.

[29] J. Lee, Y. Nam, and S. Hong, "Random force based algorithm for local minima escape of potential field method," in *Proc. 11th Int. Conf. Control Autom. Robot. Vis.*, Dec. 2010, pp. 827–832.

[30] J. Suh, H. Chae, and K. Yi, "Stochastic model-predictive control for lane change decision of automated driving vehicles," *IEEE Trans. Veh. Technol.*, vol. 67, no. 6, pp. 4771–4782, Jun. 2018.

[31] H. Min, X. Wu, C. Cheng, and X. Zhao, "Kinematic and dynamic vehicle model-assisted global positioning method for autonomous vehicles with low-cost GPS/camera/in-vehicle sensors," *Sensors*, vol. 19, no. 24, p. 5430, Dec. 2019.

[32] J. Ji, A. Khajepour, W. W. Melek, and Y. Huang, "Path planning and tracking for vehicle collision avoidance based on model predictive control with multiconstraints," *IEEE Trans. Veh. Technol.*, vol. 66, no. 2, pp. 952–964, Feb. 2017.
[33] W. Liu, A. Khajepour, H. He, H. Wang, and Y. Huang, "Integrated torque vectoring control for a three-axle electric bus based on holistic cornering control method," *IEEE Trans. Veh. Technol.*, vol. 67, no. 4, pp. 2921–2933, Apr. 2018.
[34] H. J. Ferreau, C. Kirches, A. Potschka, H. G. Bock, and M. Diehl, "QpOASES: A parametric active-set algorithm for quadratic programming," *Math. Program. Comput.*, vol. 6, no. 4, pp. 327–363, Dec. 2014.
[35] P. Wang, S. Gao, L. Li, B. Sun, and S. Cheng, "Obstacle avoidance path planning design for autonomous driving vehicles based on an improved artificial potential field algorithm," *Energies*, vol. 12, no. 12, p. 2342, Jun. 2019.

BING LU received the M.S. degree from the School of Mechanical and Vehicular Engineering, Beijing Institute of Technology, Beijing, China, in 2015, where he is currently pursuing the Ph.D. degree in mechanical engineering with the National Engineering Laboratory for Electric Vehicles. His current research interests include dynamics modeling and simulation, path planning, and tracking control for intelligent electrified vehicles.

GUOFA LI (Member, IEEE) received the Ph.D. degree in mechanical engineering from Tsinghua University, Beijing, China, in 2016. He is currently an Assistant Professor in mechanical engineering and automation with the College of Mechatronics and Control Engineering, Shenzhen University, China. His research interests include driving safety in autonomous vehicles, driver behavior and decision making, computer vision, machine learning, and human factors in automotive and transportation engineering. He was a recipient of the NSK Sino-Japan Outstanding Paper Prize from NSK Ltd., in 2014, the Excellent Young Engineer Innovation Award from SAE-China, in 2017, and the Young Elite Scientists Sponsorship Program from SAE-China, in 2018.

HUILONG YU (Member, IEEE) received the M.Sc. degree in mechanical engineering from the Beijing Institute of Technology, Beijing, China, and the Ph.D. degree in mechanical engineering from the Politecnico di Milano, Milano, Italy, in 2013 and 2017, respectively. He is currently a Research Fellow of Advanced Vehicle Engineering with the University of Waterloo, Waterloo, ON, Canada. His research interests include vehicle dynamics, optimal control, closed loop control, and energy management problems of conventional, electric, hybrid electric, and autonomous vehicles.

HONG WANG received the Ph.D. degree from the Beijing Institute of Technology, China, in 2015. From 2015 to 2019, she holds a postdoctoral position with the University of Waterloo. She is currently an Associate Research Professor with the School of Vehicle and Mobility, Tsinghua University. Her research interests include path planning control and ethical decision making for autonomous vehicles and component sizing, modeling of hybrid powertrains, and power management control strategies for hybrid electric vehicles.

JINQUAN GUO received the Ph.D. degree from the School of Mechanical Engineering, Beijing Institute of Technology, Beijing, China. From 2018 to 2019, he was a Visiting Researcher with the Department of Mechanical and Mechatronics Engineering, University of Waterloo, Waterloo, ON, Canada. He is currently holding a postdoctoral position with the School of Mechanical Engineering, Beijing Institute of Technology. His research interests include vehicle energy management and vehicle networking.

DONGPU CAO received the Ph.D. degree from Concordia University, Canada, in 2008. He is currently an Associate Professor with the Department of Mechanical and Mechatronics Engineering, University of Waterloo, Waterloo, ON, Canada. His research interests include vehicle dynamics, control, and intelligence, where he has contributed more than 90 articles and one U.S. patent. He was a recipient of the ASME AVTT 2010 Best Paper Award and the 2012 SAE Arch T. Colwell Merit Award. He serves as an Associate Editor for IEEE TRANSACTIONS ON INTELLIGENT TRANSPORTATION SYSTEMS, IEEE TRANSACTIONS ON VEHICULAR TECHNOLOGY, and IEEE TRANSACTIONS ON INDUSTRIAL ELECTRONICS. He also serves on the SAE International Vehicle Dynamics Standards Committee.

HONGWEN HE (Senior Member, IEEE) received the M.E. degree from the Jilin University of Technology, Changchun, China, in 2000, and the Ph.D. degree from the Beijing Institute of Technology, Beijing, China, in 2003, both in vehicle engineering. He is currently a Professor with the National Engineering Laboratory for Electric Vehicles, School of Mechanical Engineering, Beijing Institute of Technology. He has published more than 100 articles and holds nine patents. His research interests include power battery modeling and simulation on electric vehicles, design, and control theory of the hybrid power train. He received the First Prize of the Henan Science and Technology Award for the work on the development of hybrid bus powertrain, in 2013, the First Prize of the Henan Science and Technology Award for the work on the development of battery electric bus powertrain, in 2014, and the Second Prize of the Chinese National Science and Technology Award for the work on the development of new energy electric bus powertrains, in 2015.